Research Article

Experimental and numerical modeling of sidewall orifices

Weiping Cheng[1] · Yongxin Shen[1] · Gang Xu[2]

Received: 19 February 2020 / Accepted: 31 March 2020 / Published online: 10 April 2020

Abstract

The discharge coefficient of an orifice is important for the outflow through the orifice. While it cannot be quantified theoretically as the outflow through an orifice depends on a number of parameters such as the pipe pressure, the liquid velocity and the shape and the area of the orifice. In this study, experiments and computational fluid dynamics (CFD) simulations were performed to find out the factors influencing discharge coefficient and the corresponding mechanism. The CFD simulation is based on Navier–Stokes equations combined with RNG $k-\varepsilon$ turbulence model. The results show that a negative exponential function could fit the relationship between orifice discharge coefficient, pipe pressure, and orifice area more accurately. The relationship between the discharge coefficient of the orifice and the velocity was linear. In general, the simulation results fit well with the experimental results, which indicates that CFD simulation could be used to study pipeline leakage.

Keywords Outflow · Orifice · Velocity · Pressure · Numerical model · Computational fluid dynamics (CFD)

Abbreviations

Q_{total}	The inlet flow rate, m^3/s
Q_{out}	The outflow rate, m^3/s
Q_{end}	The outlet flow rate, m^3/s
A_{cross}	The area of the cross-section, m^2
k_a	The ration of the orifice area which represents the relative size of the orifice area
H_1	The upstream water head, m
P_a	Atmospheric pressure, P_a
ρ	The water density, kg/m^3
g	The gravity constant, 9.8 m/s^2
α_0	The kinetic energy correction factor of the inlet flow
v_{come}	The upstream velocity, m/s
P_{out}	The pressure of the shrinkage section out of the orifice, P_a
α_{out}	The kinetic energy correction factor of the orifice outflow
h_w	Local head loss, m
h_f	Frictional head loss, m
μ	Discharge coefficient of orifices
H_0	The outflow pressure in the pipeline, m
F_1	The surface tension
σ	The water surface tension coefficient
l	The perimeter of the orifice
α	The contact angle of the pipe wall
h_1	The change of the water head
A	Pipe section area, m^2
k_h	$k_h = \frac{H}{d}$
d	The pipe diameter, m
k_v	$k_v = \frac{v}{\sqrt{gd}}$
v	The velocity, m/s
k_a	$k_a = \frac{A_{out}}{A}$
A_{out}	The orifice area, m^2
$\kappa_a, \kappa_h, \kappa_v, \xi_a, \xi_h, \theta_h, \theta_v, \kappa'_h, \kappa'_v, \kappa_{vh}, \kappa_{h1}, \xi_{h1}$	Coefficients that are all positive numbers

✉ Weiping Cheng, chengweiping@zju.edu.cn; Yongxin Shen, syx_zju@zju.edu.cn; Gang Xu, 46502388@qq.com | [1]Department of Hydraulic Engineering, Zhejiang University, Hangzhou 310058, Zhejiang, People's Republic of China. [2]Guangzhou Water Supply Co., Ltd., Guangzhou 510600, People's Republic of China.

SN Applied Sciences (2020) 2:873 | https://doi.org/10.1007/s42452-020-2658-7

μ'	The discharge coefficient of the orifice of Model II
$\chi_h, \lambda_h, \chi_a, \lambda_a, \eta, \phi, \omega$	Positive coefficients
$\overline{u_i}, \overline{u_j}$	The average velocities in different coordinate axis, m/s
S_t	The source item
G_k	The turbulence production caused by the mean velocity gradient
G_b	The turbulence production caused by the buoyancy
Y_M	The influence of the compressible turbulent flow pulsation expansion on the total dissipation rate
$\alpha_k, \alpha_\varepsilon$	Respectively the reciprocal of the effective turbulent Prandtl number of turbulence energy k and dissipation rating ε
H	$(H_1+H_2)/2$

1 Introduction

Orifice outflow is a common hydrodynamic phenomenon that occurs in various industries such as the chemical industry, energy engineering, agricultural irrigation, and hydraulic engineering. Particularly, the safety of the current urban water supply network, suffering from frequent incidents of pipe leakage and explosion, is a very serious problem. Thus, in order to effectively reduce water leakage in the pipe network, it is necessary to establish models diagnosing water leakage and controlling water pressure. To this end, the discharge coefficient in the orifice outflow model must be determined.

Orifice outflow in a pipe is influenced by the pressure, the velocity, the area, and the shape of the orifice. Goodwin, Hiki, and May found that the outflow of water increased with pressure [1–3]. However, the discharge coefficient was not considered in their model. Germanopoulos et al. made up for this oversight by introducing the discharge coefficient related to the pressure to their model [4, 5].

In the field of urban water supply, empirical formulas have often been utilized to describe pipeline leakage. For example, the discharge coefficient of the point model in China is 0.421, while the coefficient of the model proposed by Shinozuka equals 0.64. Thus, the discharge coefficients used in leakage models differ significantly and cannot accurately describe the leakage situation [6, 7].

Lateral velocity prevents liquid from turning at the edge of an orifice, resulting in flow separation at the orifice. Heggeman et al. found that orifice flow in a liquid distributor was influenced by lateral velocity [8]. Through a series of pipe section simulation experiments, Jia studied leakage under different pipe diameters, pressures and leakage areas. This result showed that the influence of water pressure and leakage area on leakage was interrelated, and their relationship was described by an 'S' model [9]. The study of Prohaska et al. indicated that as the ratio of the orifice diameter to pipe diameter increased, the discharge coefficient decreased and eventually reached an asymptotic value with respect to the riser pipe [10]. And the discharge coefficient is lower for the lager pipe with the other same variables. Yu found that the discharge coefficient decreased with an increase in lateral flow velocity in the trough of a filled tower [11]. The lateral flow might lead to large-scale maldistribution in trough-type liquid distributors with larger throughput. Investigating the flow characteristics of a liquid distributor could help to avoid large-scale maldistribution. Astaraki's showed that when the length–width ratio of a rectangular opening was larger, the turbulence generated at a corner had less effect on flow reduction [12].

In this paper, to study the influence of pressure, velocity, area, and orifice shape on the orifice outflow an orifice outflow experiment with replaceable pipe sections was conducted. and the orifice outflow in a pipe was also assessed through a computational fluid dynamics (CFD) simulation. The fluid flow in the leakage pipeline includes the free flow in the pipeline and the flow through the leakage orifice. Therefore, the numerical model applied to the CFD simulation is based on Navier–Stokes equations combined with RNG k-ε turbulence model. The results show that the experimental data perfectly match the CFD simulation data. While experiments are expensive due to the costs of experimental setup, CFD simulations can be performed relatively easily. Moreover, CFD simulations have been employed to solve hydraulic engineering problems successfully. Hence, developing a simulation which is capable of reflecting the results of actual experiments is of great practical value [13–18]. The models presented in this paper could be potentially applied in engineering applications, such as leak control in the water supply industry, filled-tower optimization in the chemical industry, and drip irrigation design in agricultural irrigation.

1.1 Experimental equipment and method

1.1.1 Experimental equipment

The purpose of the experiment is to investigate the influences of the pressure and velocity of water, the orifice area, and the orifice shape on the orifice discharge coefficient. To this end, an experiment setup which is able to simulate the physical flow state and process of an orifice outflow was designed as schematically displayed in Fig. 1.

In the experimental setup, the upper water tank provided the inflow condition, and a collecting water tank was under the orifice. The water in the collecting water tank would flow into flume 1, while the downstream water would flow into flume two at the end of the pipe. The water in the flumes would flow back to the lower water tank. The water in the lower tank could be pumped back to the upper tank. In order to collect and measure the outlet flow rate and the terminal flow rate of the pipe, measuring cylinders were placed in flume 1 and 2. Piezometer tubes were used to measure the upstream and downstream pressure of the orifice in the experimental equipment.

Ghazali found that the relationship between flux and pressure was related to the shape of an orifice [19]. A replaceable pipe section was thus adopted in this experiment to explore the orifice shape effects. Valves were provided on the upstream and downstream sides of the orifice to control the working conditions. To obtain high accuracy, the mass method was used to measure the flow data.

Pipes with a variety of orifice shapes, including oval, semi-oval and a small circle, were used in this experiment (Fig. 2). The arc directions of semi-oval 1 and semi-oval 2 were different (assuming the ratio of the long axis to the short axis of the oval is 2:1). In the experiment, the shape and the area of the orifice was determined by a replaceable pipe section, as shown in Fig. 3. The length of the replaceable section was more than 20 times the pipe diameter, and thus the normal outflow would be unaffected by the fluctuation flow at the interface of the sections.

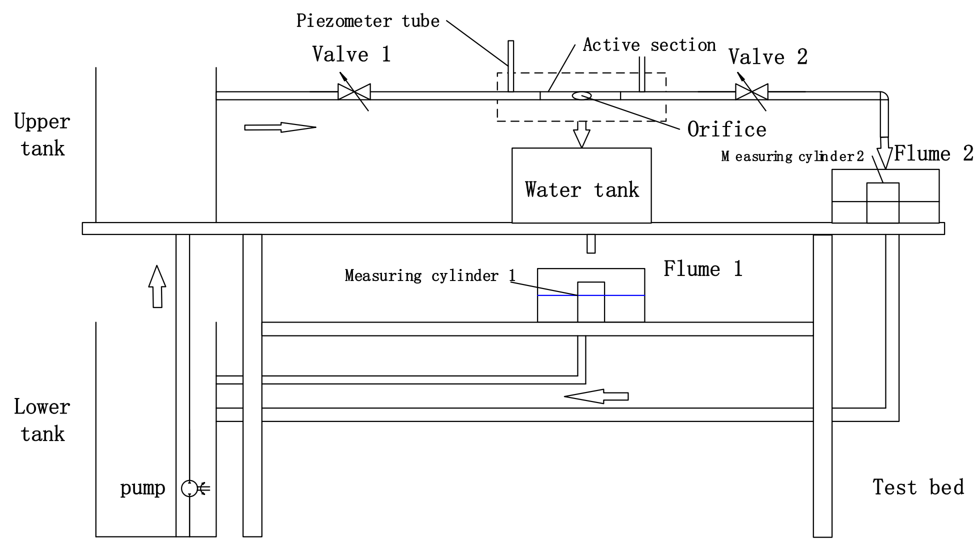

Fig. 1 Experiment setup to investigate pipe section leakage

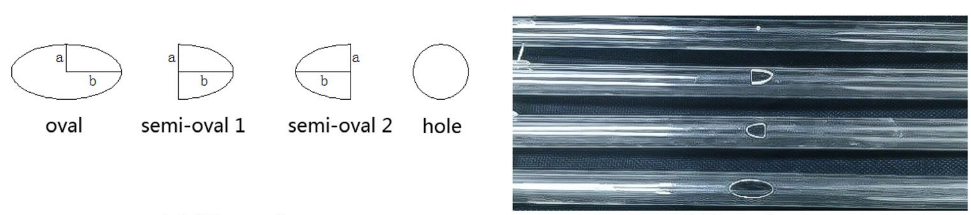

(a) Illustration **(b)** Test photo

Fig. 2 The shape of the orifice

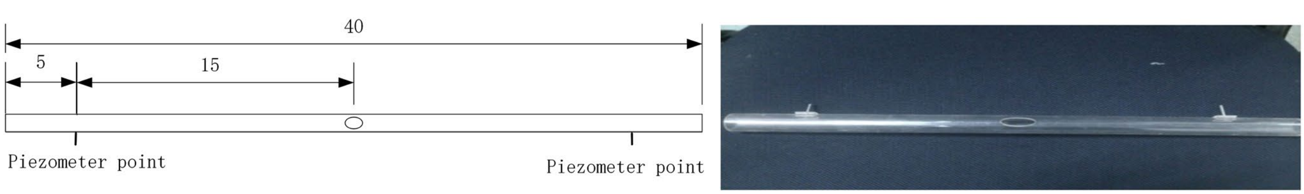

(a) Illustration **(b)** Test photo

Fig. 3 The active oval section

1.1.2 Experimental method

The experiments with different hydraulic conditions of the orifice were performed according to the following procedures.

Step 1: the pressure, the area, and the shape of orifice were set to be constant, while the velocities were altered by adjusting the valves upstream and downstream of the orifice to study the change of the outflow rate. In this step, pressure, outflow rate and flow rate at the end of the pipe were recorded.

Step 2: under constant orifice area and orifice shape, experiments using different pressures were conducted. The pressures were 2.35 cm, 2.85 cm, and 3.35 cm when the shape of the orifice was oval (except under the condition when the orifice area ratio k_a is 10%). The pressures were 2.35 cm, 2.85 cm, 3.35 cm and 6.85 cm when the shape of the orifice was oval, and the orifice area ratio k_a is 10%. When the shape of the orifice is semi-oval 1 and semi-oval 2, the pressures were 2.35 cm, 2.85 cm and 3.85 cm. When the shape of the orifice was a small circle and the orifice area ratio k_a was 2.8×10^{-3}, the pressures were 7.55 cm, 8.35 cm, and 9.35 cm. When the shape of the orifice was a small circle, and the orifice area ratio k_a was 0.11, the pressures were 6.85 cm, 7.55 cm, and 8.35 cm. Step 1 should be repeated for every pressure.

Step 3: with a constant orifice shape, experiments using different orifice areas were conducted. When the orifice shape was oval, the orifice area ratios k_a were 10%, 20%, 40%, 60%, and 80%. When the orifice shape was semi-oval 1, the orifice area ratios k_a were 20%, 30%, and 40%. When the orifice shape was semi-oval 2, the orifice area ratio k_a was 40%. When the shape was a small circle, the orifice area ratios k_a were 2.8×10^{-3} and 0.011. Steps 1 and 2 should be repeated for every orifice area.

Step 4: experiments using different orifice shapes were conducted. Steps 1, 2 and 3 were repeated for different orifice shapes (oval, semi-oval 1, semi-oval 2 and circle).

In this experiment, the main measurements are the pressure (upstream and downstream), the orifice outflow rate and the terminal flow rate. The total pipeline flow is calculated by the orifice outflow rate and the flow rate at the end of the pipe. The formula is as follows:

$$Q_{total} = Q_{out} + Q_{end} \tag{1}$$

$$v_{come} = Q_{total}/A_{cross} \tag{2}$$

The detailed experimental conditions are present in Table 1.

1.2 Establishment of models and data analysis

1.2.1 Theoretical analysis of orifice outflow characteristics

To analyze and discuss experimental results, a theoretical explanation of orifice outflow characteristics is given. As Fig. 4 shows, when the upstream water flows through the orifice, a certain amount of flow would leak through the orifice, and the rest continues downstream. The flow lines in the section through the orifice are unparallel, and thus the water flow continues to shrink until the flow lines become parallel. This section is called the shrinkage section outside the orifice. The shrinkage factor ε is the ratio of the shrinkage section area to the outflow rate section area.

The energy Eq. (3) between the orifice cross-section and upstream cross-section is established according to the Bernoulli equation. The equation can be expressed as:

$$H_1 + \frac{p_a}{\rho g} + \frac{\alpha_0 v_{come}^2}{2g} = \frac{p_{out}}{\rho g} + \frac{\alpha_{out} v_{come}^2}{2g} + h_w + h_f \tag{3}$$

where H_1 is the upstream water head (m), P_a is atmospheric pressure (P_a), v_{come} is upstream velocity (m/s), P_{out} is the pressure of the shrinkage section out of the orifice (P_a), v_{out} is the average velocity of the shrinkage section out of the orifice (m/s), h_w is local head loss (m), and h_f is frictional head loss (m). Assuming that the water head of the orifice outflow is $H_0 = H_1 + \frac{\alpha_0 v_{come}^2}{2g} - h_f$, an equation for the outflow rate can be expressed as follows:

$$Q_{out} = \mu A_{out}\sqrt{2gH_0} \tag{4}$$

where A_{out} is orifice area (m^2), Q_{out} is outflow rate (m^3/s), H_0 is the outflow pressure in the pipeline (m); μ is the discharge coefficient of the orifice, and its value is usually 0.60–0.62. However, the outflow in a pipe or a channel with a transverse flow is significantly different from a general orifice discharge. When the orifice is small, the effect of the surface tension on discharge is great. This effect of the surface tension on the outflow rate is described as follows.

$$F_1 = \sigma \cdot l \cdot \cos\alpha \tag{5}$$

where F_1 is the surface tension, σ is the water surface tension coefficient, l is the perimeter of the orifice; α is the contact angle of the pipe wall.

The variation in the water head (h_1) can be described as follows:

$$h_1 = \frac{F_1}{\rho g A} = \frac{\sigma \cdot l \cdot \cos\beta}{\rho g A} \tag{6}$$

The impact of the surface tension on the outflow pressure is also expressed by $\frac{h_1}{H_0}$.

Table 1 The experimental conditions

Condition	Shape of orifice	Outflow area ratio k_a	Average pressure upstream and downstream at the measuring point H (cm)	Remarks
Condition 1	Oval	10%	2.35	Axial ratio of 2:1
			2.85	
			3.35	
			6.85	
Condition 2	Oval	20%	2.35	
			2.85	
			3.35	
Condition 3	Oval	40%	2.35	
			2.85	
			3.35	
Condition 4	Oval	60%	2.35	
			2.85	
			3.35	
Condition 5	Oval	80%	2.35	
			2.85	
			3.35	
Condition 6	Semi-oval 1	20%	2.85	
			3.35	
			3.85	
Condition 7	Semi-oval 1	30%	2.85	
			3.35	
			3.85	
Condition 8	Semi-oval 1	40%	2.85	
			3.35	
			3.85	
Condition 9	Semi-oval 2	40%	2.85	
			3.35	
			3.85	
Condition 10	Small circle	2.8×10^{-3}	7.55	
			8.35	
			9.35	
Condition 11	Small circle	0.011	6.85	
			7.55	
			8.35	

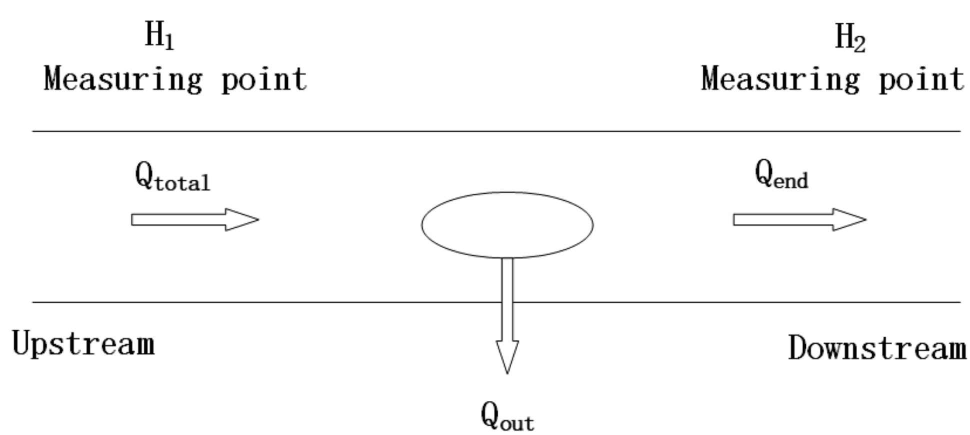

Fig. 4 The flow conditions at the orifice point

To satisfy the needs of research, three dimensionless numbers, namely k_h, k_v, and k_a, were introduced.

$$k_h = \frac{H}{d} \tag{7}$$

where k_h is the ratio of the pressure to the pipe diameter and represents the average pressure; H (m) is defined as the average of H_1 and H_2, i.e., $(H_1 + H_2)/2$, and d (m) stands for the pipe diameter.

$$k_v = \frac{v}{\sqrt{gd}} \tag{8}$$

where k_v is the flow velocity, and v (m/s) represents the velocity of water; d (m) denotes the section diameter.

$$k_a = \frac{A_{leak}}{A} \tag{9}$$

where k_a is the ratio of the orifice area and represents the relative size of the orifice; A_{out} and A (m^2) indicate the orifice area and pipe section area, respectively.

Computational results indicate that the impact of surface tension on the total head is less than 5% with a k_a greater than 0.2, while the impact on the outflow rate is relatively large, up to 22%, with a k_a less than 0.2.

The equation for the outflow rate is $Q_{leak} = \mu A_{out}\sqrt{2g(H_0 - h_1)}$. The effect of surface tension on the value of Q_{out} is less than 5%, which can be ignored in most engineering situations. Therefore, ignoring the effect of surface tension would likely not influence the results of this experiment.

1.3 Data analysis and fitting

According to the experimental data, there is a negative linear relationship between the discharge coefficient of the orifice (μ) and the velocity, as shown in Fig. 5. A linear function could be used to describe the relationship between the discharge coefficient of the orifice (μ) and the velocity.

In Fig. 5a–c, different fitting curves correspond to the oval, semi-oval 1 and semi-oval 2 orifices, the orifice area of which are the same. This illustrates that the orifice shape influences the discharge coefficient of an orifice.

Figure 6 shows that μ increases with k_a and k_h, and the relationship tends to slow. This indicates that there is a positive correlation in how μ is affected by the orifice area and the pressure.

Figure 5 indicates that μ is influenced by the shape of the orifices, which means the equation of the model changes with the shape of the orifice. This study focused

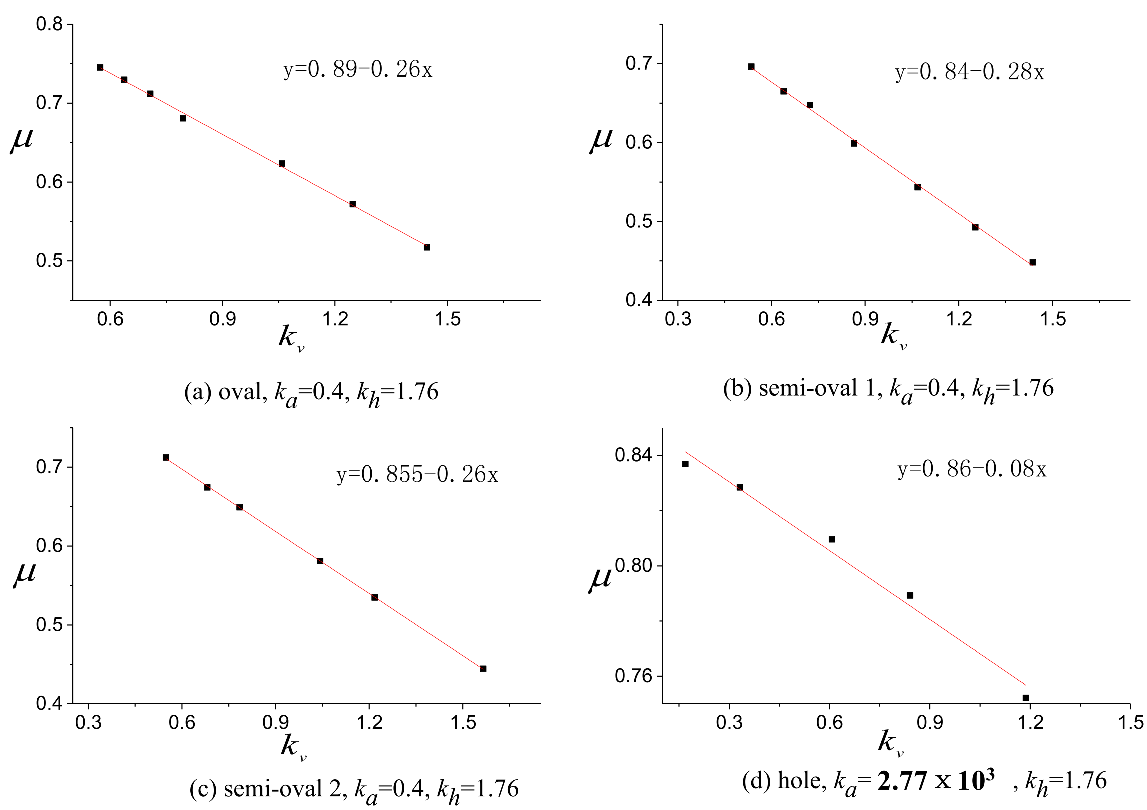

Fig. 5 The change of μ with k_v in different orifices

Fig. 6 The change of μ with k_a and k_h

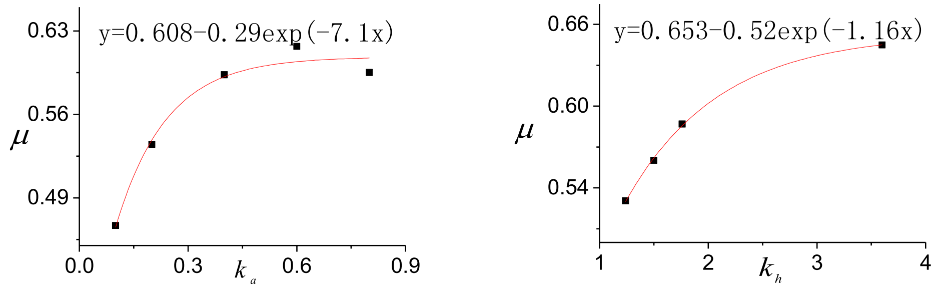

(a) oval, k_h=1.76, k_v=1.16, the change of μ with k_a (b) oval, k_a=0.1, k_v=0.46, the change of μ with k_h

on the equation of the oval orifice, which is called the oval orifice Model I.

1.4 The establishment of oval orifice Model I

As pipeline pressure increases, it gradually becomes the main factor affecting orifice outflow. If the outflow rate loss caused by a transverse flow can be neglected, then the value of μ should approach 1. With a gradual increase in the orifice area, it can be seen from the Fig. 6a that the value of μ is gradually approaching 1. Therefore, a negative exponential function could describe the relationship between orifice discharge coefficient, pipe pressure, and orifice area more accurately. Combined with the linear relationship between the discharge coefficient of the orifice and the velocity, the relationship between μ, k_h, k_v and k_a is as follows:

$$\mu = (1 - \kappa_a e^{-\xi_a k_a}) \cdot [\theta_h \cdot (1 - \kappa_h e^{-\xi_h k_h})] \cdot [\theta_v \cdot (1 - \kappa_v k_v)] \tag{10}$$

where κ_a, κ_v, κ_h, ξ_a, ξ_v, ξ_h are coefficients that are all positive numbers. Because the upper limit of μ is 1, Eq. (10) can be developed into:

$$\mu = (1 - \kappa_a e^{-\xi_a k_a}) \cdot (1 - \kappa_h' e^{-\xi_h k_h} - \kappa_v' k_v + \kappa_{vh} k_v \cdot e^{-\xi_h k_h}) \tag{11}$$

where κ_h', κ_v' and κ_{vh} are coefficients that are positive numbers.

Equation (4) shows that μ is mainly influenced by the upstream pressure H_1; Thus κ_h could be replaced by κ_{h1} ($k_{h1} = H_1/d$), which represents the upstream pressure. The equation is developed as follows:

$$\mu = (1 - \kappa_a e^{-\xi_a k_a}) \cdot (1 - \kappa_{h1} e^{-\xi_{h1} k_{h1}} - \kappa_v' k_v + \kappa_{vh1} k_v \cdot e^{-\xi_{h1} k_{h1}}) \tag{12}$$

where κ_{h1}, ξ_{h1} and κ_{vh1} are positive coefficients.

After using the experimental data in the case of the oval orifice to fit Model I, a unified equation can be obtained as follows:

$$\mu = (1 - 0.5e^{-5.6k_a}) \cdot (1 - 0.37e^{-k_{h1}} - 0.2k_v - 0.32k_v \cdot e^{-k_{h1}}) \tag{13}$$

The multiple correlation coefficient R^2 of Model I is 0.997. Figure 7 shows the degree of curve fitting.

Combined with Eq. (13), Eq. (2) can be developed into orifice outflow Model I.

$$Q_{out} = (1 - 0.5e^{-5.6k_a}) \cdot (1 - 0.37e^{-k_{h1}} - 0.2k_v - 0.32k_v \cdot e^{-k_{h1}}) A_{out}\sqrt{2gH_0} \tag{14}$$

Note that Model I has some limitations. Under conditions of high velocity and low pressure, the real outflow rate stops. But in Model I, the outflow rate is always greater than zero. Also, the computational process is relatively complicated because it needs to measure the upstream velocity in the pipe.

1.5 The establishment of Model II

The linear correlation of $\frac{Q_{out}}{Q_{total}}$ and $\frac{A_{out}\sqrt{2gH}}{Q_{total}}$ can be seen in Fig. 8. The relationship between the outflow rate, the

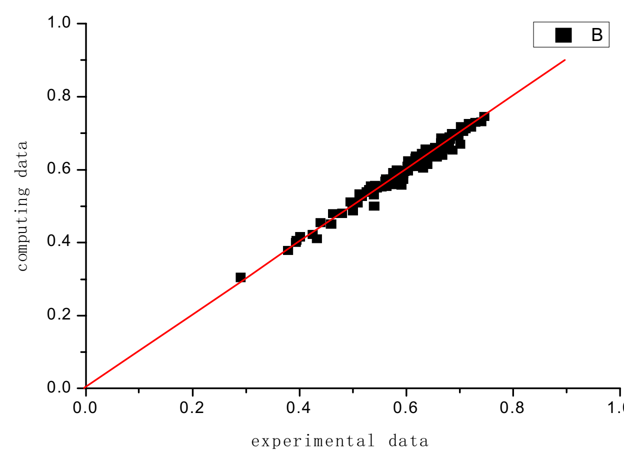

Fig. 7 The distribution map of computing data and experimental data

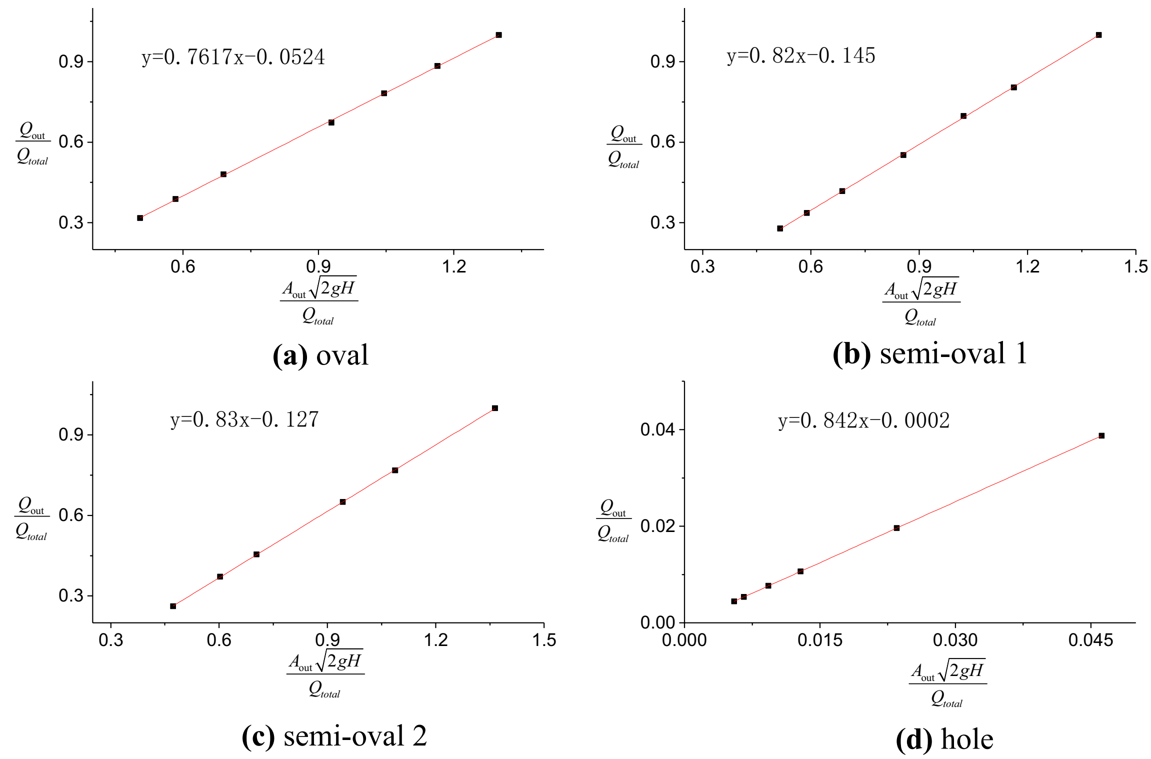

Fig. 8 $k_a = 0.4$, $k_h = 1.76$, the change of $\frac{Q_{out}}{Q_{total}}$ with $\frac{A_{out}\sqrt{2gH}}{Q_{total}}$

orifice area, the pressure, and the total flow rate is as follows:

$$Q_{out} = \mu' A_{out}\sqrt{2gH} - \alpha Q_{total} \tag{15}$$

The above equation is Model II. μ' is the discharge coefficient of the orifice of Model II. αQ_{total} measures the influence of the horizontal flow on the outflow of lateral orifices, and α is the effective coefficient of the lateral orifices.

Orifice outflow Model II is also the equation of the oval orifice outflow. Figure 9a and b show the relationship curve of μ', k_a and k_h in Model II. Figure 9c shows the relationship curve of α and k_a.

Figure 9a and b indicate that μ' has a positive correlation with k_a and k_h, and the rising trend gradually slows. Figure 9c shows that α increases with k_a, and the rising trend gradually accelerates, which reflects the relationship between α and the orifice area.

Orifice Model II could be described as follows:

$$Q_{out} = (1 - \chi_h e^{-\lambda_h k_h}) * (1 - \chi_a e^{-\lambda_a k_a}) \cdot A_{leak}\sqrt{2gH} - (\eta e^{\phi k_a} - \omega)Q \tag{16}$$

where χ_h, λ_h, χ_a, λ_a, η, Φ, and ω are positive coefficients, A is the orifice area(m^2), H is the orifice pressure (m), and Q is the total flow rate (m^3/s). After using the experimental data of the oval orifice to fit Model II, an equation could be obtained as follows:

$$Q_{leak} = (1 - 0.215e^{-6.3k_h}) \cdot (1 - 0.44e^{-4.1k_a}) \cdot A_{leak}\sqrt{2gH} - [0.12(e^{1.67k_a}) - 0.117]Q \tag{17}$$

The multiple correlation coefficient R^2 of Model II is 0.999, which shows the simulation results fit the experimental data well. This model could be used to describe the relationship between μ' and other factors accurately and conveniently.

1.6 CFD simulation

1.6.1 The principle of the CFD model

Orifice outflow of a pipe includes free flow in the pipe and flow at the orifice. Assuming that the flow is incompressible, the governing equations of the flow are obtained by using continuity equations and Navier–Stokes equations:

$$\frac{\partial \rho \overline{u_i}}{\partial x_i} = 0 \tag{18}$$

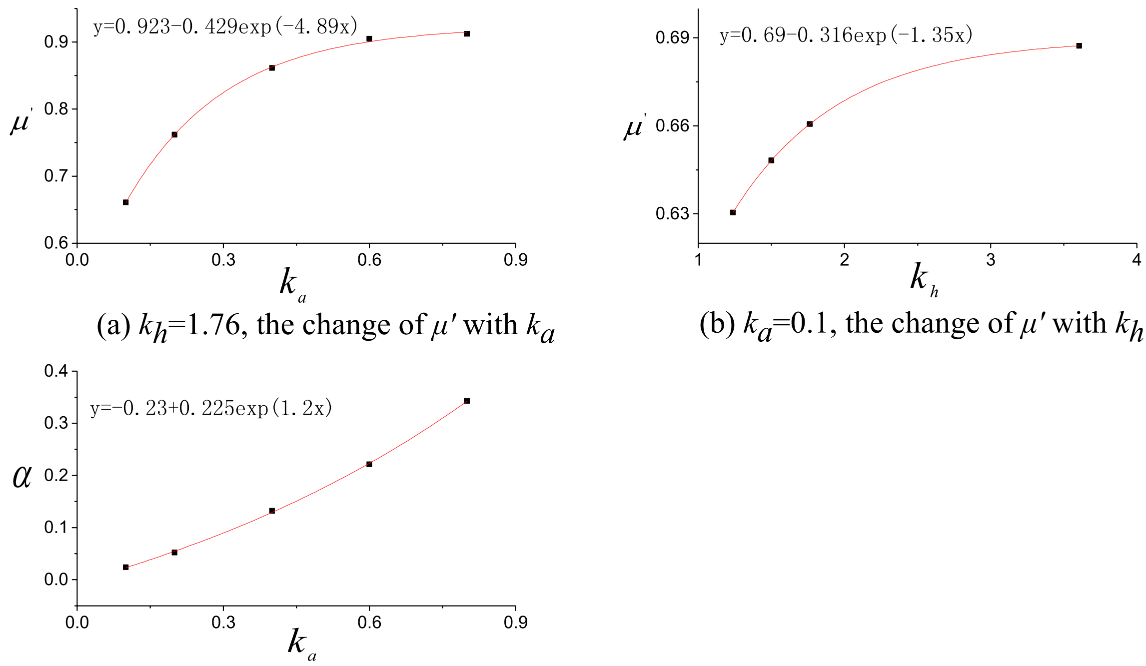

(a) k_h=1.76, the change of μ' with k_a

(b) k_a=0.1, the change of μ' with k_h

(c) k_h=1.76, the change of α with k_a

Fig. 9 The change of μ' and α with k_a and k_h

$$\frac{\partial}{\partial t}(\rho\overline{u_i}) + \frac{\partial \rho\overline{u_i u_j}}{\partial x_i} = -\frac{\partial p}{\partial x_i} + \mu\frac{\partial^2 \overline{u_i}}{\partial x_i x_j} - \frac{\partial(\rho\overline{u_i u_j})}{\partial x_i} + S_t \tag{19}$$

where ρ is the density of the fluid, $\overline{u_i}$ and $\overline{u_j}$ are the average velocities in different coordinate axes, p is the pressure and $\rho\overline{u_i u_j}$ is the Reynolds stress. S_t is the source term.

The governing equation of the renormalization $k-\varepsilon$ model is as follows:

$$\rho\frac{dk}{dt} = \frac{\partial}{\partial x_i}\left[(\alpha_k\mu_{\text{eff}})\frac{\partial k}{\partial x_i}\right] + G_k + G_b - \rho\varepsilon - Y_M \tag{20}$$

$$\rho\frac{d\varepsilon}{dt} = \frac{\partial}{\partial x_i}\left[(\alpha_g\mu_{\text{eff}})\frac{\partial \varepsilon}{\partial x_i}\right] + C_{1\varepsilon}\frac{\varepsilon}{k}(G_k + G_{3g}G_b) - C_{2s}\rho\frac{\varepsilon^2}{k} - R \tag{21}$$

where G_k is the turbulent kinetic energy due to the average velocity gradient, G_b is the turbulent kinetic energy due to buoyancy and Y_M is the effect of the fluctuating expansion of the compressible turbulent flow on the total dissipation rate. These parameters are the same as those in the standard $k-\varepsilon$ model. α_k and α_ε are reciprocals of the turbulent kinetic energy k and the effective Prandtl number of the dissipation rate ε, respectively.

The formula for calculating the turbulent viscous coefficient is as follows:

$$d\left(\frac{\rho^2 k}{\sqrt{\varepsilon\mu}}\right) = 1.72\frac{\tilde{v}}{\sqrt{\tilde{v}^3 - 1 - Cv}}d\tilde{v} \tag{22}$$

where $\tilde{v} = \frac{\mu e_{eff}}{\mu}$ and $C_v = 100$.

The renormalization group $k-\varepsilon$ model could accurately predict the effect of the effective Reynolds number (vortex viscosity) on turbulent transport, which is helpful for the simulation of low-Reynolds number and near-wall flows. For high Reynolds numbers, Eq. (22) could be given as: $\mu_t = \rho C_\mu \frac{k^2}{\varepsilon}, C_\mu = 0.0845$. This result is very close to the semi-empirical constant derivation from the standard $k-\varepsilon$ model, $C_\mu = 0.09$ (Fig. 10).

1.6.2 The establishment of the CFD model

This study simulated Model I and Model II by experimental and numerical simulation, so the computing domain of the model was set according to the experimental equipment. The computing domain and the grid are shown in Fig. 11.

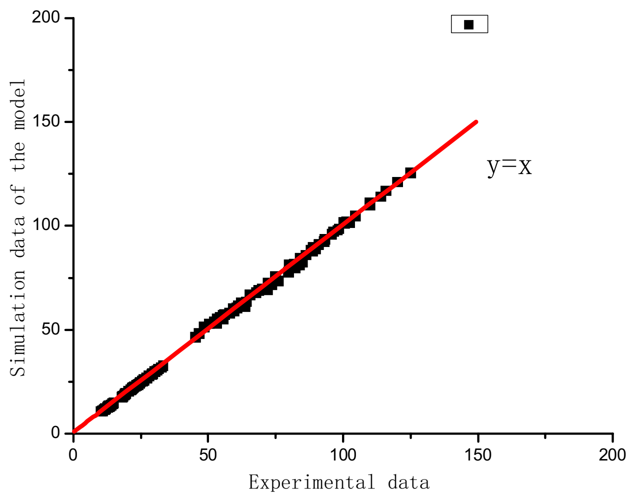

Fig. 10 The distribution map of simulation data of the model and experimental data

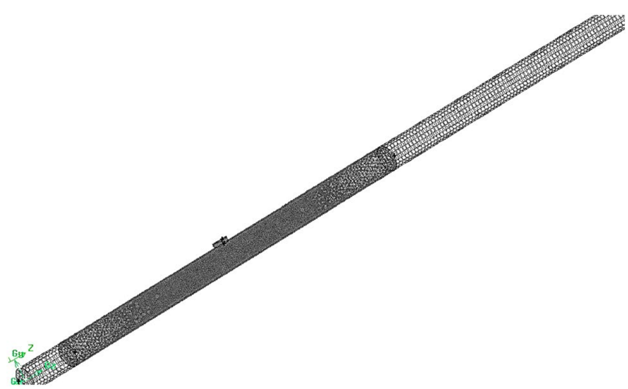

Fig. 11 The computing domain of the CFD model

The computing domain was a circular tube (570 mm long, 19 mm diameter and 3 mm thickness). The center of the orifice was 38 mm away from the upstream flow. The medium in the computing domain was the water of 25° Centigrade, and the boundary conditions at the import and the export of the model were both velocity inlet. The boundary condition at the orifice was pressure outlet. As the water at the outflow hole was exposed to the atmosphere, the pressure value was set to 0. The boundary conditions at the piezometric surfaces of both sides were interior. The boundary conditions at other surfaces were set as well, which was no slip walls with velocities of 0. In the computing field, Hex grid was adopted at the piezometric surfaces of both sides and the two ends, while the rest of the area used Tet grid. The grid at the orifice was finer to make the description of flow conditions more precise.

1.6.3 Comparison of the simulation and experimental results

The experimental data and the simulation results under the same conditions of pressures and orifice areas are compared in the curve of $\mu - k_v$, as shown in Figs. 12, 13, 14, 15 and 16. The curves of experimental data and simulation results fit well with a deviation of less than 10% (except for Fig. 15). The experimental data curve trend was generally consistent with the simulation curve, which indicated that CFD could precisely describe the influence of velocities on the orifice discharge coefficient. Figure 15 presents the experimental data and results of the simulation have the biggest deviation. This is mainly because the surface tension and viscous force had a great effect on the outflow at the orifice when the orifice area ratio was 10%.

2 Discussion and conclusion

To investigate the effect of velocities on the outflow rate, a piece of self-designed equipment was used to simulate an orifice outflow under different pressures, orifice areas, and shapes. After analysis, the relationships between outflow rate and pressure, velocities, orifice areas, and shapes were determined. The experimental results indicate that the discharge coefficient of an orifice (μ) could be affected by velocities, pressures, orifice areas, and orifice shape. Specifically, μ had a negative linear correlation with velocity, increased with orifice area and pressure, and the relationships tended to slow as μ increases. Oval orifice outflow Model I was obtained based on the experiment results.

Combined with the analysis of experiment results and data fitting, oval orifice outflow Model II was established, which could accurately describe the relationships between μ and pressure, velocity, and orifice area.

The effects of velocities on the outflow rate under different pressures and orifice areas could be obtained through CFD simulation to analyze the flow condition at

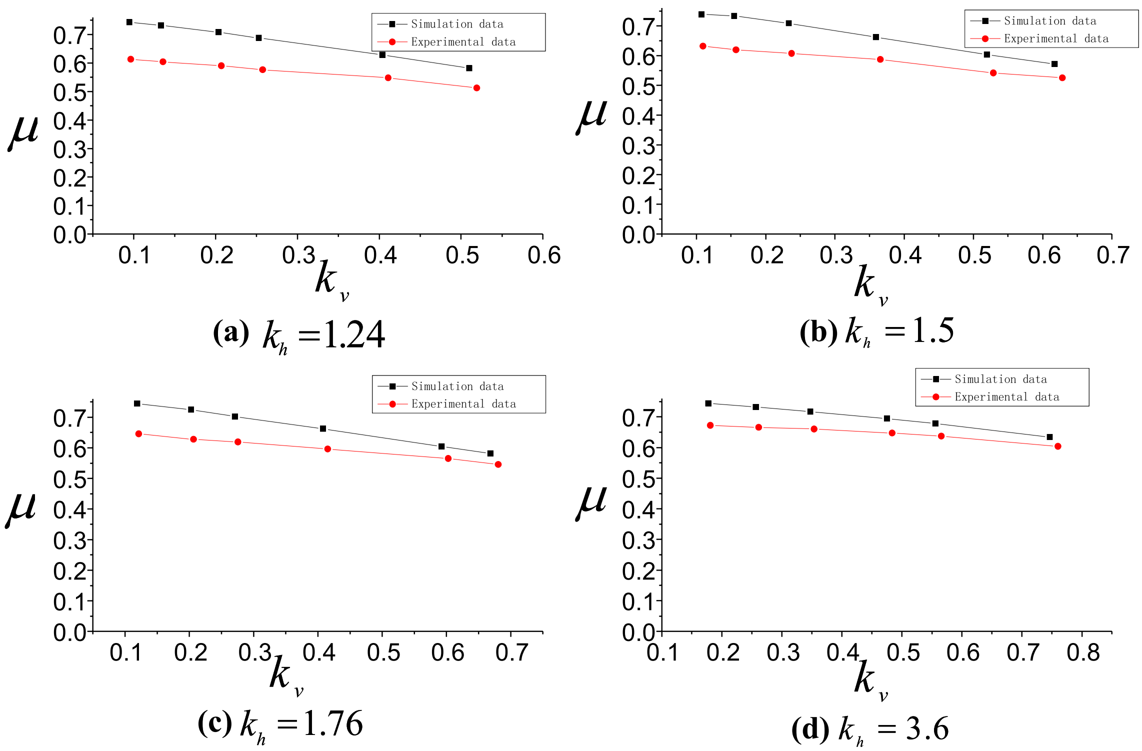

Fig. 12 The $\mu - k_v$ curve in the orifice area ratio of 10%

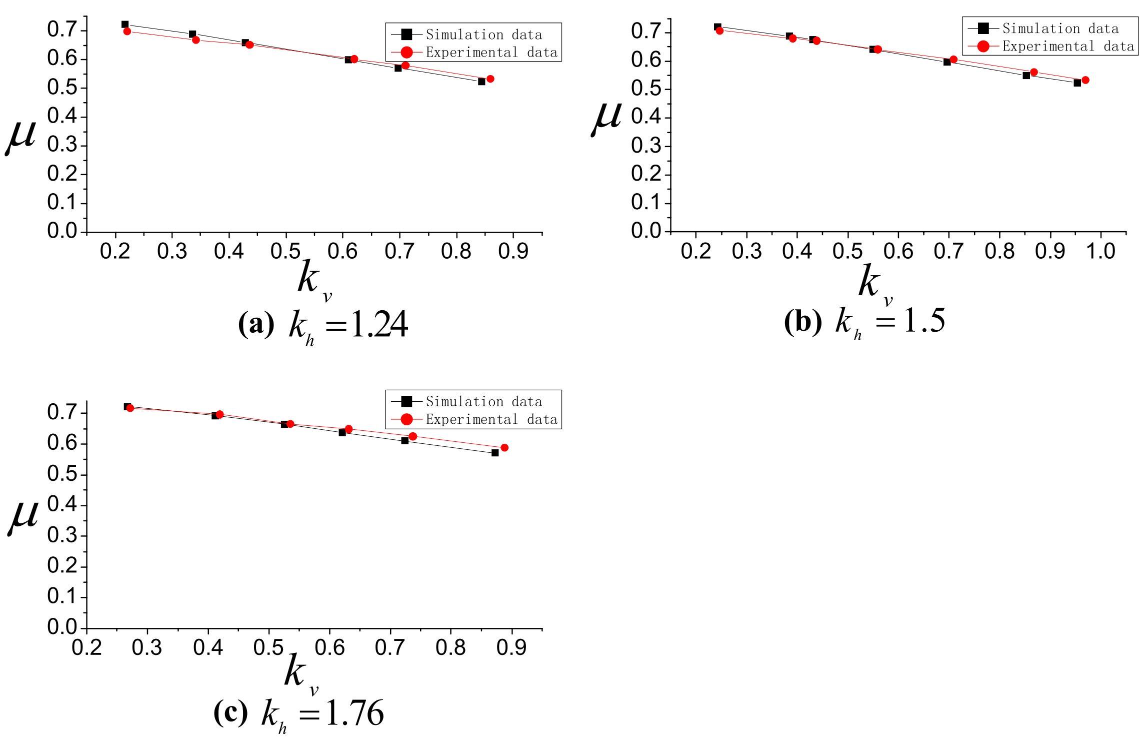

Fig. 13 The $\mu - k_v$ curve in the orifice area ratio of 20%

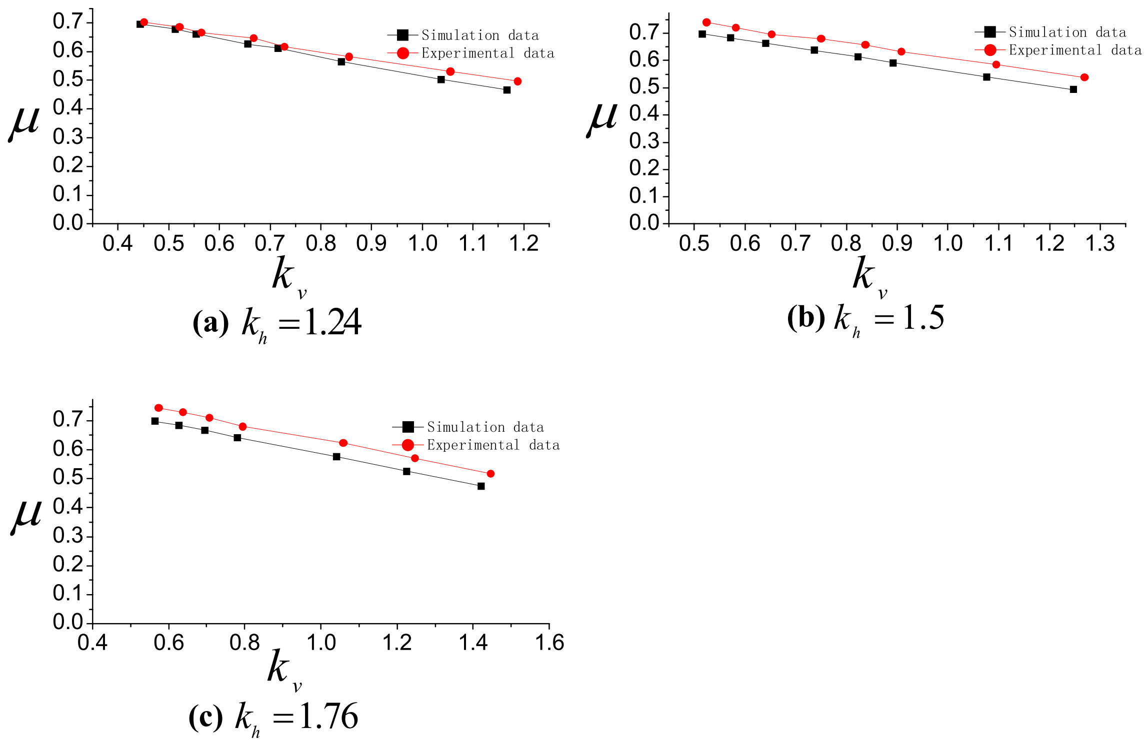

Fig. 14 The $\mu - k_v$ curve in the orifice area ratio of 40%

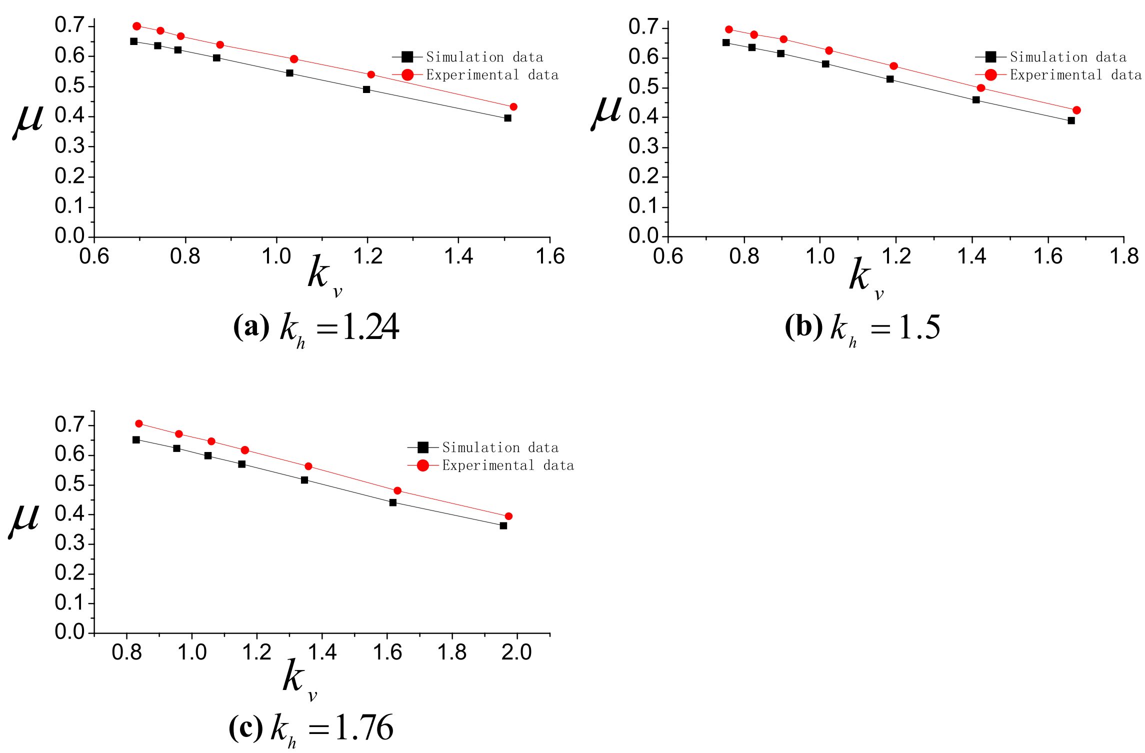

Fig. 15 The $\mu - k_v$ curve in the orifice area ratio of 60%

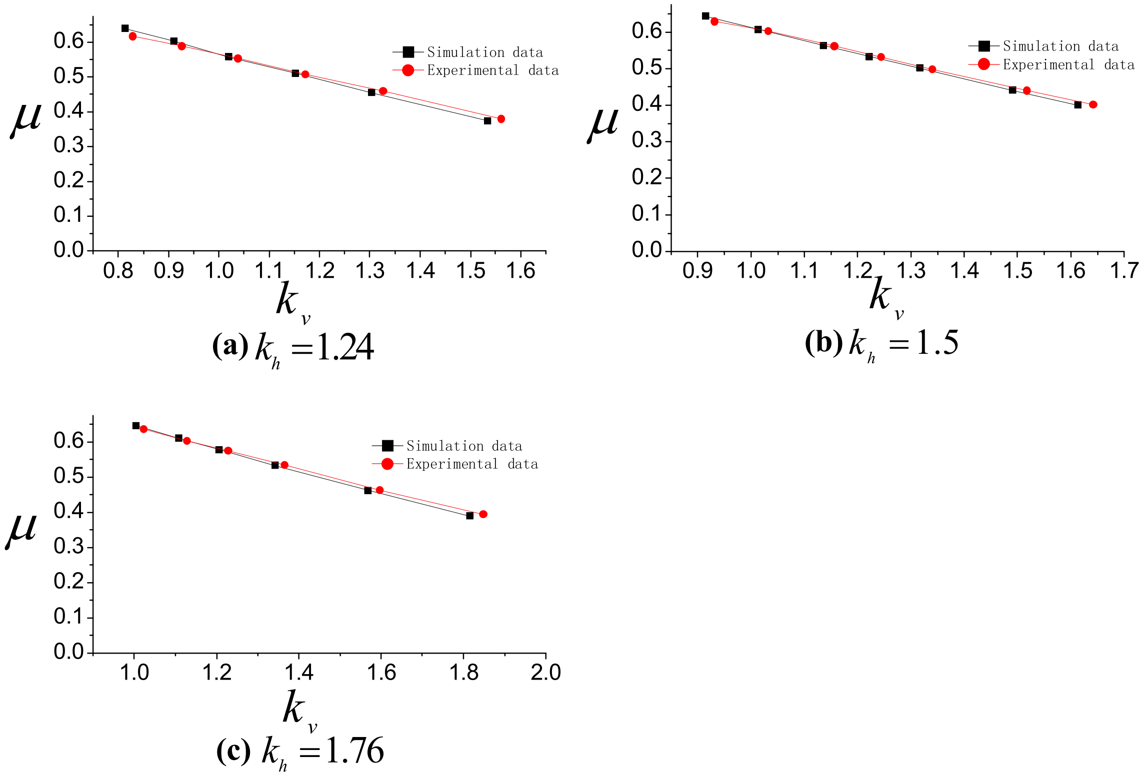

Fig. 16 The $\mu - k_v$ curve in the orifice area ratio of 80%

the orifice. The simulation results were consistent with the experiment results, which could prove the accuracy of the experiment and shows that the CFD simulation could accurately describe the effect of velocities on the orifice outflow in the pipe.

The results show that when the leak area is large (leakage area ratio k_a is greater than 20%), CFD simulations and experimental results would have small deviations. While when the leak area is small, the two would have large deviations. This is mainly because when the leak area is small, the experimental results could be affected by viscous force, surface tension, and leak cutting errors. The simulated results matched well with the experimental results in general, indicating that CFD simulation could be potentially used to study actual water supply pipeline leakage.

Compliance with ethical standards

Conflict of interest The authors declare that they have no conflicts of interest.

Appendix: Experimental data and analysis results

The shape of the crack	Q_{out}	Q_{total}	v	H_1	H_2	H	H_0	k_a	μ	$\frac{Q_{out}}{Q_{total}}$	$\frac{A_{out}\sqrt{gH}}{Q_{total}}$	Re
Oval	27.07	27.07	0.096	2.36	2.34	2.35	2.39	0.2	0.697	1	1.42415	1802
	26.16	41.82	0.148	2.36	2.34	2.35	2.43	0.2	0.669	0.625	0.92163	2784
	25.69	53.29	0.188	2.35	2.35	2.35	2.47	0.2	0.651	0.482	0.72179	3548
	24.42	75.86	0.268	2.36	2.34	2.35	2.62	0.2	0.602	0.322	0.50815	5050
	23.96	86.79	0.306	2.37	2.33	2.35	2.71	0.2	0.58	0.276	0.44507	5778
	22.96	105.1	0.371	2.44	2.26	2.35	2.95	0.2	0.533	0.219	0.37309	6994
	30.2	30.2	0.107	2.85	2.85	2.85	2.89	0.2	0.708	1	1.40265	2010
	29.27	47.83	0.169	2.85	2.85	2.85	2.95	0.2	0.68	0.612	0.88556	3184
	29.07	53.6	0.189	2.85	2.85	2.85	2.97	0.2	0.672	0.542	0.79031	3568
	28.11	68.41	0.241	2.85	2.85	2.85	3.06	0.2	0.641	0.411	0.6192	4554
	27.22	86.62	0.306	2.86	2.84	2.85	3.2	0.2	0.607	0.314	0.48988	5766
	26.09	106.2	0.375	2.9	2.8	2.85	3.42	0.2	0.562	0.246	0.4024	7069
	25.44	118.6	0.419	2.95	2.75	2.85	3.61	0.2	0.534	0.214	0.36326	7898
	33.2	33.2	0.117	3.35	3.35	3.35	3.4	0.2	0.717	1	1.38331	2210
	32.49	51.25	0.181	3.35	3.35	3.35	3.46	0.2	0.696	0.634	0.89608	3412
	31.4	65.5	0.231	3.35	3.35	3.35	3.54	0.2	0.665	0.479	0.70116	4360
	30.98	77.21	0.272	3.35	3.35	3.35	3.62	0.2	0.649	0.401	0.59478	5140
	30.24	90.11	0.318	3.35	3.35	3.35	3.72	0.2	0.625	0.336	0.50967	5999
	29.22	108.6	0.383	3.37	3.33	3.35	3.92	0.2	0.589	0.269	0.42419	7229
	55.28	55.28	0.195	2.33	2.37	2.35	2.46	0.4	0.702	1	1.38579	3680
	54.46	63.79	0.225	2.33	2.37	2.35	2.51	0.4	0.685	0.854	1.20083	4247
	53.25	69.02	0.244	2.33	2.37	2.35	2.54	0.4	0.666	0.772	1.10989	4595
	52.13	81.7	0.288	2.28	2.42	2.35	2.58	0.4	0.647	0.638	0.92746	5439
	50.36	89.07	0.314	2.28	2.42	2.35	2.64	0.4	0.618	0.565	0.85078	5929
	48.57	104.6	0.369	2.26	2.44	2.35	2.76	0.4	0.582	0.464	0.72121	6964
	46.54	129.1	0.455	2.27	2.43	2.35	3.05	0.4	0.531	0.361	0.58583	8592
	45.24	145.2	0.512	2.3	2.4	2.35	3.3	0.4	0.496	0.312	0.52411	9667

The shape of the crack	Q_{out}	Q_{total}	v	H_1	H_2	H	H_0	k_a	μ	$\frac{Q_{out}}{Q_{total}}$	$\frac{A_{out}\sqrt{gH}}{Q_{total}}$	Re
	37.87	213.5	0.753	2.45	2.25	2.35	4.68	0.4	0.349	0.177	0.36799	14,210
	64.12	64.12	0.226	2.8	2.9	2.85	2.98	0.4	0.74	1	1.30957	4269
	62.95	71.12	0.251	2.8	2.9	2.85	3.02	0.4	0.721	0.885	1.18074	4734
	61.18	79.75	0.281	2.78	2.92	2.85	3.06	0.4	0.696	0.767	1.04924	5309
	60.6	91.67	0.323	2.77	2.93	2.85	3.15	0.4	0.68	0.661	0.91113	6102
	59.41	102.4	0.361	2.76	2.94	2.85	3.24	0.4	0.657	0.58	0.81412	6817
	57.81	111.1	0.392	2.73	2.97	2.85	3.3	0.4	0.634	0.52	0.74648	7395
	55.47	134	0.473	2.71	2.99	2.85	3.56	0.4	0.586	0.414	0.61659	8919
	53.06	155.2	0.548	2.7	3	2.85	3.85	0.4	0.539	0.342	0.53126	10,333
	44.77	224.5	0.792	2.85	2.85	2.85	5.32	0.4	0.387	0.199	0.37732	14,947
	70.14	70.14	0.248	3.3	3.4	3.35	3.52	0.4	0.745	1	1.29973	4669
Oval	68.91	77.97	0.275	3.27	3.43	3.35	3.54	0.4	0.73	0.884	1.16384	5191
	67.67	86.5	0.305	3.25	3.45	3.35	3.59	0.4	0.712	0.782	1.04585	5759
	65.47	97.23	0.343	3.24	3.46	3.35	3.67	0.4	0.681	0.673	0.92903	6473
	62.23	129.5	0.457	3.17	3.53	3.35	3.96	0.4	0.623	0.481	0.68989	8622
	59.23	152.6	0.538	3.15	3.55	3.35	4.26	0.4	0.572	0.388	0.58379	10,156
	56.13	176.8	0.624	3.17	3.53	3.35	4.68	0.4	0.517	0.317	0.50526	11,772
	48.97	243.8	0.86	3.35	3.35	3.35	6.29	0.4	0.389	0.201	0.37668	16,233
	84.79	84.79	0.299	2.26	2.44	2.35	2.58	0.6	0.701	1	1.33468	5644
	83.71	91.21	0.322	2.25	2.45	2.35	2.63	0.6	0.686	0.918	1.23797	6072
	82.05	96.59	0.341	2.24	2.46	2.35	2.67	0.6	0.667	0.849	1.16645	6430
	79.87	107.1	0.378	2.23	2.47	2.35	2.76	0.6	0.639	0.746	1.04959	7130
	76.03	127	0.448	2.16	2.54	2.35	2.92	0.6	0.591	0.599	0.87111	8455
	71.97	147.7	0.521	2.1	2.6	2.35	3.14	0.6	0.54	0.487	0.73868	9831
	63.56	185.9	0.656	2.13	2.57	2.35	3.8	0.6	0.433	0.342	0.59096	12,376
	53.83	242.3	0.855	2.26	2.44	2.35	5.16	0.6	0.315	0.222	0.46705	16,130
	92.87	92.87	0.328	2.74	2.96	2.85	3.13	0.6	0.697	1	1.34175	6182
	91	101.1	0.357	2.7	3	2.85	3.17	0.6	0.679	0.9	1.22349	6730
	89.64	110.6	0.39	2.65	3.05	2.85	3.22	0.6	0.664	0.81	1.10795	7363
	86.17	125.2	0.442	2.62	3.08	2.85	3.35	0.6	0.625	0.688	0.97313	8335
	81.74	146	0.515	2.57	3.13	2.85	3.58	0.6	0.574	0.56	0.82635	9722
	74.97	174.1	0.614	2.5	3.2	2.85	3.96	0.6	0.5	0.431	0.68379	11,587
	68.57	204.9	0.723	2.55	3.15	2.85	4.6	0.6	0.425	0.335	0.58667	13640
	57.24	287.2	1.014	2.84	2.86	2.85	6.95	0.6	0.288	0.199	0.44167	19,121

The shape of the crack	Q_{out}	Q_{total}	v	H_1	H_2	H	H_0	k_a	μ	$\frac{Q_{out}}{Q_{total}}$	$\frac{A_{out}\sqrt{gH}}{Q_{total}}$	Re
	102.4	102.4	0.361	3.23	3.47	3.35	3.71	0.6	0.706	1	1.32146	6815
	98.47	117.5	0.414	3.14	3.56	3.35	3.78	0.6	0.673	0.838	1.13561	7819
	95.73	129.5	0.457	3.07	3.63	3.35	3.86	0.6	0.647	0.739	1.01822	8623
	93.06	142.1	0.502	3.05	3.65	3.35	4.01	0.6	0.618	0.655	0.92493	9462
	87.96	166.1	0.586	2.99	3.71	3.35	4.31	0.6	0.563	0.53	0.78364	11,058
	80	199.6	0.704	2.96	3.74	3.35	4.9	0.6	0.48	0.401	0.64885	13,287
	72.1	241.3	0.852	3.05	3.65	3.35	5.92	0.6	0.394	0.299	0.54473	16,066
	61.93	310.2	1.095	3.28	3.42	3.35	8.1	0.6	0.289	0.2		20,650
	101.3	101.3	0.357	2.2	2.5	2.35	2.67	0.8	0.617	1	1.47007	6741
	97.87	113.2	0.4	2.15	2.55	2.35	2.75	0.8	0.589	0.864	1.29961	7538
	93.18	126.9	0.448	2.06	2.64	2.35	2.82	0.8	0.553	0.734	1.13534	8447
	88.61	143.3	0.506	2.04	2.66	2.35	3.01	0.8	0.508	0.618	1.00005	9543
	82.9	162.2	0.573	1.97	2.73	2.35	3.23	0.8	0.459	0.511	0.86825	10,801
	73.63	190.9	0.674	1.97	2.73	2.35	3.74	0.8	0.379	0.386	0.73791	12,709
	60.83	242.2	0.855	2.14	2.56	2.35	5.03	0.8	0.27	0.251	0.60628	16,122
	113.9	113.9	0.402	2.65	3.05	2.85	3.25	0.8	0.629	1	1.4349	7580
	110	126.1	0.445	2.56	3.14	2.85	3.31	0.8	0.603	0.872	1.27316	8397
	104.5	141.3	0.499	2.5	3.2	2.85	3.45	0.8	0.561	0.739	1.12272	9410
	100.7	152.1	0.537	2.45	3.25	2.85	3.55	0.8	0.532	0.662	1.0329	10,125
	96.57	163.9	0.578	2.43	3.27	2.85	3.72	0.8	0.499	0.589	0.95443	10,913
Oval	89.03	185.6	0.655	2.4	3.3	2.85	4.07	0.8	0.44	0.48	0.83779	12,355
	84.1	200.8	0.709	2.38	3.32	2.85	4.34	0.8	0.402	0.419	0.77112	13,367
	70.66	258.9	0.914	2.55	3.15	2.85	5.87	0.8	0.291	0.273	0.61894	17,238
	125	125	0.441	3.1	3.6	3.35	3.83	0.8	0.636	1	1.41367	8322
	120.2	138	0.487	3.03	3.67	3.35	3.93	0.8	0.604	0.871	1.26578	9188
	115.9	150.2	0.53	2.95	3.75	3.35	4.02	0.8	0.576	0.772	1.14795	9997
	109.8	167	0.589	2.85	3.85	3.35	4.19	0.8	0.534	0.657	1.01479	11,115
	100.3	195.2	0.689	2.8	3.9	3.35	4.65	0.8	0.463	0.514	0.8602	12,997
	90.86	225.9	0.797	2.76	3.94	3.35	5.27	0.8	0.394	0.402	0.73799	15,041
	76.13	291.4	1.028	2.95	3.75	3.35	7.19	0.8	0.283	0.261	0.59159	19,399
Semi-oval 1	29.9	29.9	0.106	2.85	2.85	2.85	2.89	0.2	0.701	1	1.41658	1991
	29.4	35.34	0.125	2.85	2.85	2.85	2.91	0.2	0.687	0.832	1.1988	2352
	29.07	41.37	0.146	2.85	2.85	2.85	2.92	0.2	0.678	0.703	1.02396	2754
	28.37	51.84	0.183	2.84	2.86	2.85	2.95	0.2	0.658	0.547	0.81573	3451
	27.57	63.53	0.224	2.84	2.86	2.85	3.02	0.2	0.633	0.434	0.66558	4229
	26.07	84.01	0.296	2.85	2.85	2.85	3.17	0.2	0.584	0.31	0.50424	5592
	24.17	109.6	0.387	2.89	2.81	2.85	3.45	0.2	0.519	0.221	0.38932	7294

The shape of the crack	Q_{out}	Q_{total}	v	H_1	H_2	H	H_0	k_a	μ	$\frac{Q_{out}}{Q_{total}}$	$\frac{A_{out}\sqrt{gH}}{Q_{total}}$	Re
	22.63	136.1	0.48	2.95	2.75	2.85	3.82	0.2	0.461	0.166	0.31668	9060
	32.97	32.97	0.116	3.35	3.35	3.35	3.4	0.2	0.712	1	1.39303	2195
	32.2	39.17	0.138	3.35	3.35	3.35	3.41	0.2	0.695	0.822	1.17257	2607
	31.7	47.73	0.168	3.35	3.35	3.35	3.44	0.2	0.681	0.664	0.96218	3177
	31.4	52.97	0.187	3.34	3.36	3.35	3.46	0.2	0.673	0.593	0.86575	3526
	30.54	66.97	0.236	3.33	3.37	3.35	3.53	0.2	0.648	0.456	0.68368	4458
	29.7	78.07	0.275	3.33	3.37	3.35	3.6	0.2	0.624	0.38	0.58653	5197
	28.23	95.18	0.336	3.35	3.35	3.35	3.76	0.2	0.58	0.297	0.48251	6336
	27.3	110.1	0.388	3.36	3.34	3.35	3.92	0.2	0.549	0.248	0.41785	7328
	24.37	157.6	0.556	3.55	3.15	3.35	4.74	0.2	0.446	0.155	0.30004	10,489
	35.4	35.4	0.125	3.85	3.85	3.85	3.91	0.2	0.713	1	1.3907	2357
	34.93	43.43	0.153	3.85	3.85	3.85	3.93	0.2	0.702	0.804	1.13358	2891
	34.4	54.4	0.192	3.84	3.86	3.85	3.97	0.2	0.688	0.632	0.90382	3622
	32.58	73.24	0.258	3.82	3.88	3.85	4.06	0.2	0.645	0.445	0.6696	4876
	31.07	95.87	0.338	3.84	3.86	3.85	4.26	0.2	0.6	0.324	0.51287	6382
	28.6	128.9	0.455	3.87	3.83	3.85	4.65	0.2	0.528	0.222	0.38286	8583
	27.33	146.4	0.517	3.95	3.75	3.85	4.97	0.2	0.489	0.187	0.34064	9746
	43.16	43.16	0.152	2.85	2.85	2.85	2.93	0.3	0.67	1	1.47235	2873
	42.42	51.79	0.183	2.84	2.86	2.85	2.95	0.3	0.656	0.819	1.22474	3448
	41.47	62.8	0.222	2.83	2.87	2.85	3	0.3	0.636	0.66	1.00825	4181
	39	84.6	0.299	2.8	2.9	2.85	3.12	0.3	0.586	0.461	0.74444	5632
	36.04	110.8	0.391	2.84	2.86	2.85	3.41	0.3	0.519	0.325	0.57239	7377
	32.71	143.1	0.505	2.86	2.84	2.85	3.83	0.3	0.444	0.229	0.4449	9524
	47.09	47.09	0.166	3.35	3.35	3.35	3.44	0.3	0.674	1	1.46295	3135
	46.22	54.32	0.192	3.33	3.37	3.35	3.46	0.3	0.661	0.851	1.26436	3616
	45.44	59.44	0.21	3.3	3.4	3.35	3.45	0.3	0.65	0.765	1.15026	3957
Semi-oval 1	43.87	75.74	0.267	3.3	3.4	3.35	3.55	0.3	0.618	0.579	0.90277	5042
	41.09	99.03	0.349	3.3	3.4	3.35	3.75	0.3	0.564	0.415	0.69042	6593
	38.47	122.3	0.432	3.3	3.4	3.35	4	0.3	0.511	0.315	0.55908	8141
	35.13	158.8	0.56	3.36	3.34	3.35	4.57	0.3	0.437	0.221	0.43437	10574
	50.09	50.09	0.177	3.85	3.85	3.85	3.96	0.3	0.669	1	1.4744	3334
	49.62	59.76	0.211	3.8	3.9	3.85	3.95	0.3	0.663	0.83	1.22783	3978
	49.2	66.2	0.234	3.77	3.93	3.85	3.96	0.3	0.657	0.743	1.10395	4407
	47.27	82.97	0.293	3.76	3.94	3.85	4.07	0.3	0.623	0.57	0.87967	5523
	45.16	100.5	0.355	3.75	3.95	3.85	4.21	0.3	0.584	0.449	0.72528	6690
	42.04	128.8	0.455	3.77	3.93	3.85	4.55	0.3	0.524	0.326	0.56731	8575
	38.36	163.9	0.578	3.86	3.84	3.85	5.15	0.3	0.449	0.234	0.45122	10,910

The shape of the crack	Q_{out}	Q_{total}	v	H_1	H_2	H	H_0	k_a	μ	$\frac{Q_{out}}{Q_{total}}$	$\frac{A_{out}\sqrt{gH}}{Q_{total}}$	Re
	60.93	60.93	0.215	2.89	2.81	2.85	3.05	0.4	0.695	1	1.4001	4056
	58.13	78.16	0.276	2.84	2.86	2.85	3.11	0.4	0.657	0.744	1.08198	5203
	55.69	91.49	0.323	2.8	2.9	2.85	3.18	0.4	0.622	0.609	0.91783	6091
	50.67	123.6	0.436	2.77	2.93	2.85	3.49	0.4	0.541	0.41	0.67573	8228
	49.2	134.6	0.475	2.76	2.94	2.85	3.62	0.4	0.516	0.365	0.61923	8963
	45.64	160.2	0.565	2.8	2.9	2.85	4.03	0.4	0.453	0.285	0.52403	10668
	65.53	65.53	0.231	3.33	3.37	3.35	3.52	0.4	0.696	1	1.39741	4363
	62.8	78.07	0.275	3.27	3.43	3.35	3.54	0.4	0.665	0.804	1.16239	5197
	61.69	88.46	0.312	3.25	3.45	3.35	3.6	0.4	0.648	0.697	1.02276	5889
	58.29	105.6	0.373	3.25	3.45	3.35	3.76	0.4	0.599	0.552	0.85646	7032
	54.56	130.7	0.461	3.2	3.5	3.35	4	0.4	0.543	0.418	0.68708	8698
	51.56	153.2	0.541	3.23	3.47	3.35	4.35	0.4	0.493	0.336	0.58862	10200
	48.96	175.7	0.62	3.25	3.45	3.35	4.74	0.4	0.448	0.279	0.51492	11,696
	69.67	69.67	0.246	3.83	3.87	3.85	4.04	0.4	0.69	1	1.40974	4638
	66.07	89.93	0.317	3.75	3.95	3.85	4.12	0.4	0.649	0.735	1.08059	5987
	63.42	105.9	0.374	3.73	3.97	3.85	4.25	0.4	0.613	0.599	0.91562	7047
	60.47	124.7	0.44	3.7	4	3.85	4.43	0.4	0.573	0.485	0.7741	8301
	57.87	142.5	0.503	3.7	4	3.85	4.66	0.4	0.534	0.406	0.67739	9487
	53.2	179.1	0.632	3.73	3.97	3.85	5.28	0.4	0.461	0.297	0.54117	11923
Semi-oval 2	60.76	60.76	0.214	2.83	2.87	2.85	2.99	0.4	0.7	1	1.38954	4045
	59.44	70.22	0.248	2.8	2.9	2.85	3.02	0.4	0.682	0.847	1.19591	4674
	57.53	86.04	0.304	2.76	2.94	2.85	3.09	0.4	0.652	0.669	0.96904	5727
	55.04	105	0.37	2.75	2.95	2.85	3.26	0.4	0.608	0.524	0.79268	6989
	49.33	145.7	0.514	2.75	2.95	2.85	3.76	0.4	0.507	0.339	0.57129	9697
	45.91	171.2	0.604	2.78	2.92	2.85	4.19	0.4	0.447	0.268	0.48881	11395
	67.13	67.13	0.237	3.33	3.37	3.35	3.53	0.4	0.712	1	1.36411	4469
	63.96	83.29	0.294	3.26	3.44	3.35	3.57	0.4	0.674	0.768	1.08789	5545
	62.42	95.99	0.339	3.25	3.45	3.35	3.67	0.4	0.649	0.65	0.94247	6390
	58.04	127.5	0.45	3.2	3.5	3.35	3.96	0.4	0.581	0.455	0.70399	8489
	55.33	148.8	0.525	3.2	3.5	3.35	4.25	0.4	0.535	0.372	0.60311	9909
	50.02	191.5	0.676	3.25	3.45	3.35	5.03	0.4	0.444	0.261	0.4725	12747
	71.07	71.07	0.251	3.8	3.9	3.85	4.02	0.4	0.706	1	1.37655	4731
Semi-oval 2	69.02	83.19	0.294	3.77	3.93	3.85	4.08	0.4	0.681	0.83	1.17125	5538
	66.87	100.9	0.356	3.73	3.97	3.85	4.2	0.4	0.65	0.663	0.9609	6715
	63.84	123.5	0.436	3.7	4	3.85	4.41	0.4	0.606	0.517	0.78176	8220
	60.13	150.3	0.53	3.65	4.05	3.85	4.73	0.4	0.551	0.4	0.63776	10008
	55.58	188.9	0.667	3.7	4	3.85	5.43	0.4	0.475	0.294	0.5109	12578

The shape of the crack	Q_{out}	Q_{total}	v	H_1	H_2	H	H_0	k_a	μ	$\frac{Q_{out}}{Q_{total}}$	$\frac{A_{out}\sqrt{gH}}{Q_{total}}$	Re
Hole	0.8	20.67	0.073	7.55	7.55	7.55	7.57	0.00277	0.837	0.039	0.0462	1376
	0.797	40.63	0.143	7.6	7.5	7.55	7.67	0.00277	0.828	0.02	0.02358	2705
	0.79	74.26	0.262	7.65	7.45	7.55	7.89	0.00277	0.81	0.011	0.01294	4944
	0.787	102.8	0.363	7.74	7.36	7.55	8.23	0.00277	0.789	0.008	0.00941	6843
	0.778	145.2	0.512	7.86	7.24	7.55	8.86	0.00277	0.752	0.005	0.00671	9664
	0.769	173.9	0.614	7.95	7.15	7.55	9.41	0.00277	0.721	0.004	0.00563	11577
	0.854	28.98	0.102	8.36	8.34	8.35	8.4	0.00277	0.848	0.029	0.03467	1930
	0.848	61.08	0.216	8.45	8.25	8.35	8.61	0.00277	0.831	0.014	0.01654	4066
	0.842	92.22	0.325	8.5	8.2	8.35	8.89	0.00277	0.813	0.009	0.01099	6139
	0.839	111.1	0.392	8.55	8.15	8.35	9.12	0.00277	0.799	0.008	0.00915	7397
	0.832	145.1	0.512	8.67	8.03	8.35	9.67	0.00277	0.77	0.006	0.00705	9662
	0.826	173.2	0.611	8.75	7.95	8.35	10.2	0.00277	0.744	0.005	0.00594	11527
	0.91	28.71	0.101	9.37	9.33	9.35	9.41	0.00277	0.853	0.032	0.03705	1911
	0.905	64.14	0.226	9.45	9.25	9.35	9.63	0.00277	0.839	0.014	0.01666	4270
	0.9	99.5	0.351	9.54	9.16	9.35	9.99	0.00277	0.819	0.009	0.01079	6624
	0.894	126.8	0.447	9.6	9.1	9.35	10.4	0.00277	0.8	0.007	0.00849	8439
	0.887	167.2	0.59	9.75	8.95	9.35	11.1	0.00277	0.766	0.005	0.00649	11,128
	2.546	21.41	0.076	6.86	6.84	6.85	6.88	0.011	0.698	0.119	0.17003	1426
	2.52	44.32	0.156	6.87	6.83	6.85	6.95	0.011	0.688	0.057	0.0822	2951
	2.487	67.78	0.239	6.95	6.75	6.85	7.15	0.011	0.669	0.037	0.05407	4512
	2.429	101.4	0.358	7	6.7	6.85	7.47	0.011	0.639	0.024	0.03627	6751
	2.414	132.4	0.467	7.1	6.6	6.85	7.93	0.011	0.617	0.018	0.02798	8812
	2.369	177.9	0.628	7.24	6.46	6.85	8.77	0.011	0.575	0.013	0.02103	11843
	2.641	32.84	0.116	7.57	7.53	7.55	7.62	0.011	0.688	0.08	0.11646	2186
	2.612	45.51	0.161	7.59	7.51	7.55	7.68	0.011	0.678	0.057	0.08415	3030
	2.58	60.28	0.213	7.64	7.46	7.55	7.8	0.011	0.665	0.043	0.06375	4013
	2.571	70.8	0.25	7.65	7.45	7.55	7.87	0.011	0.659	0.036	0.0543	4714
	2.562	84.83	0.299	7.66	7.44	7.55	7.98	0.011	0.652	0.03	0.04536	5647
	2.545	95.08	0.336	7.67	7.43	7.55	8.08	0.011	0.644	0.027	0.04049	6330
	2.509	136	0.48	7.8	7.3	7.55	8.67	0.011	0.613	0.018	0.02854	9054
	2.825	28.93	0.102	8.37	8.33	8.35	8.41	0.011	0.701	0.098	0.13904	1926
	2.812	43.95	0.155	8.4	8.3	8.35	8.48	0.011	0.695	0.064	0.09168	2926
	2.772	77.54	0.274	8.45	8.25	8.35	8.72	0.011	0.675	0.036	0.05212	5162
	2.718	117.4	0.414	8.55	8.15	8.35	9.19	0.011	0.645	0.023	0.03463	7814
	2.63	187.8	0.663	8.75	7.95	8.35	10.5	0.011	0.585	0.014	0.0219	12,501

References

1. Goodwin SJ (1980) Results of the experimental programme on leakage and leakage control. In WRC technical report. WRc
2. Hiki S (1981) Relationship between leakage and pressure. J Jpn Waterworks Assoc 5:50–54
3. May J (1994) Pressure dependent leakage. World Water Environ Eng 17(8):10
4. Germanopoulos G (1985) A technical note on the inclusion of pressure dependent demand and leakage terms in water supply network models. Civ Eng Syst 2(3):171–179
5. Germanopoulos G, Jowitt PW (1989) Leakage reduction by excess pressure minimization in a water-supply network. Proc Inst Civ Eng Part 2 Res Theory 87:195–214. https://doi.org/10.1680/iicep.1989.2003
6. Lijuan W, Hongwei Z (2010) Study on leakage loss model for water distribution network. China Water Waste Water 9:68–70
7. Hwng HHM, Lin H, Shinozuka M (1998) Seismic performance assessment of water delivery systems. J Infrastruct Syst 4(3):118–125
8. Heggemann M, Hirschberg S, Spiegel L, Bachmann C (2007) CFD simulation and experimental validation of fluid flow in liquid distributors. Chem Eng Res Des 85(A1):59–64. https://doi.org/10.1205/cherd06093
9. Jia H (2008) Study on leakage hydraulic characteristics of municipal water supply network. Ph.D, Tianjin University, Cnki
10. Prohaska PD, Khan AA, Kaye NB (2010) Investigation of flow through orifices in riser pipes. J Irrig Drain Eng 136(5):340–347. https://doi.org/10.1061/(ASCE)IR.1943-4774.0000195
11. Yu H, Li X, Sui H, Xu C, Li H (2013) Simulation of orifice flow influenced by lateral flow in a trough-type liquid distributor. Chem Eng Technol 36(11):1975–1984. https://doi.org/10.1002/ceat.201300162
12. Astaraki A, Hosseini M, Soroushian A, Ghazizadeh MJ (2018) Experimental and numerical investigations on the effect of rectangular openings' aspect ratio on outflow discharge. J Appl Comput Mech 4(Special Issue: Applied and Computational Issues in Structural Engineering):457–466. https://doi.org/10.22055/jacm.2018.25519.1275
13. Parsaie A, Haghiabi AH, Moradinejad A (2015) CFD modeling of flow pattern in spillway's approach channel. Sustain Water Resour Manag 1(3):245–251. https://doi.org/10.1007/s40899-015-0020-9
14. Parsaie A, Haghiabi AH (2015) The effect of predicting discharge coefficient by neural network on increasing the numerical modeling accuracy of flow over side weir. Water Resour Manag 29(4):973–985. https://doi.org/10.1007/s11269-014-0827-4
15. Parsaie A, Dehdar-Behbahani S, Haghiabi AH (2016) Numerical modeling of cavitation on spillway's flip bucket. Front Struct Civ Eng 10(4):438–444. https://doi.org/10.1007/s11709-016-0337-y
16. Dehdar-Behbahani S, Parsaie A (2016) Numerical modeling of flow pattern in dam spillway's guide wall. Case study: Balaroud dam, Iran. Alex Eng J 55(1):467–473. https://doi.org/10.1016/j.aej.2016.01.006
17. Parsaie A, Haghiabi AH (2017) Numerical routing of tracer concentrations in rivers with stagnant zones. Water Sci Technol: Water Supply 17(3):825–834. https://doi.org/10.2166/ws.2016.175
18. Parsaie A, Moradinejad A, Haghiabi AH (2018) Numerical modeling of flow pattern in spillway approach channel. Jordan J Civ Eng 12(1):1–9
19. Ardakanian, Reza, and A. A. Ghazali (2003) Pressure-leakage relation in urban water distribution systems. In: Paper presented at the pipeline engineering and construction international conference 2003. American Society of Civil Engineers